Homoclinic orbits and chaos in a pair of parametrically driven coupled nonlinear resonators

Eyal Kenig,[1] Yuriy A. Tsarin,[2] and Ron Lifshitz[1,*]

[1]*Raymond and Beverly Sackler School of Physics and Astronomy, Tel Aviv University, Tel Aviv 69978, Israel*

[2]*Institute of Radio Astronomy, National Academy of Sciences of Ukraine, 4 Krasnoznamennya St., Kharkov 61002, Ukraine*

(Received 21 July 2010; revised manuscript received 28 January 2011; published 18 July 2011)

We study the dynamics of a pair of parametrically driven coupled nonlinear mechanical resonators of the kind that is typically encountered in applications involving microelectromechanical systems (MEMS) and nanoelectromechanical systems (NEMS). We take advantage of the weak damping that characterizes these systems to perform a multiple-scales analysis and obtain amplitude equations, describing the slow dynamics of the system. This picture allows us to expose the existence of homoclinic orbits in the dynamics of the integrable part of the slow equations of motion. Using a version of the high-dimensional Melnikov approach, developed by G. Kovačič and S. Wiggins [Physica D **57**, 185 (1992)], we are able to obtain explicit parameter values for which these orbits persist in the full system, consisting of both Hamiltonian and non-Hamiltonian perturbations, to form so-called Šilnikov orbits, indicating a loss of integrability and the existence of chaos. Our analytical calculations of Šilnikov orbits are confirmed numerically.

DOI: 10.1103/PhysRevE.84.016212 PACS number(s): 05.45.−a, 85.85.+j, 62.25.−g, 47.52.+j

I. INTRODUCTION

Microelectromechanical systems (MEMS) and nanoelectromechanical systems (NEMS) have been attracting much attention in recent years [1–3]. MEMS and NEMS resonators are typically characterized by very high frequencies, extremely small masses, and weak damping. As such, they are naturally being developed for a variety of applications such as sensing with unprecedented accuracy [4–6], and also for studying fundamental physics at small scales—exploring mesoscopic phenomena [7,8] and even approaching quantum behavior [9–11]. MEMS and NEMS resonators often exhibit nonlinear behavior in their dynamics [12,13]. This includes nonlinear resonant response showing frequency pulling, multistability, and hysteresis [3,14–17], as well as the formation of extended [18] and localized [19] collective states in arrays of coupled nonlinear resonators, and the appearance of chaotic dynamics [20–22]. Nonlinearities are often a nuisance in actual applications, and schemes are being developed to avoid them [23], but one can also benefit from the existence of nonlinearity, for example in mass-sensing applications [24,25], in suppressing noise-induced phase diffusion [26], in achieving self-synchronization of large arrays [27], and even in the observation of quantum behavior [28].

MEMS and NEMS offer a wonderful experimental testing ground for theories of chaotic dynamics. Numerical investigations of a number of models of MEMS and NEMS resonators have demonstrated period-doubling transitions to chaos [22,29–32], yet there are very few analytical results. One of the simplest models of chaotic motion is that of the Duffing resonator with a double-well potential, described by the Hamiltonian,

$$H(x,p) = \frac{1}{2m}p^2 + \frac{1}{2}kx^2 + \frac{1}{4}\alpha x^4, \qquad (1)$$

with $k < 0$ and $\alpha > 0$. This simple mechanical system has a homoclinic orbit for $H = 0$, connecting a saddle at the origin of phase space to itself. Upon the addition of damping and an external drive this system develops a particular kind of chaotic motion called *horseshoe chaos* [33], which can be studied analytically using the Melnikov approach [34]. The stable manifold leading into the saddle and the unstable manifold leading away from the saddle, which coincide in the unperturbed Hamiltonian (1), are deformed when damping and a drive are added. Yet, conditions can be found analytically using the Melnikov function, which measures the distance between the two manifolds, under which they intersect transversely leading to the possibility of observing chaotic dynamics. What one observes in practice is a random-like switching of the resonator between the two wells. Thus, having an analytical criterion for asserting the existence of chaotic motion allows one to distinguish it from random stochastic motion that might arise from noise. Such a Hamiltonian as in Eq. (1) was implemented in a MEMS device using an external electrostatic potential by DeMartini *et al.* [21], and studied using the Melnikov approach.

Here we wish to study the possibility of having horseshoe chaos in typical NEMS resonators, which are described by a potential as in Eq. (1), but of an elastic origin with k and α both positive. Individual resonators of this type do not exhibit homoclinic orbits for any value of H, and therefore are not expected to display horseshoe chaos under a simple periodic drive. Nevertheless, a pair of coupled resonators of this kind—like the ones studied experimentally by Karabalin *et al.* [22]—are shown below to possess homoclinic orbits in their collective dynamics, and are therefore amenable to analysis based on a high-dimensional version of the Melnikov approach [35]. We employ here a particular method, developed by Kovačič and Wiggins [36], which is a combination of the high-dimensional Melnikov approach and geometric singular perturbation theory. This method enables us to find conditions, in terms of the actual physical parameters of the resonators, for the existence of an orbit in four-dimensional phase space, which is homoclinic to a fixed point of a saddle-focus type.

*Corresponding author: ronlif@tau.ac.il

Such an orbit, called a Šilnikov orbit [33,37], provides a mechanism for producing chaotic dynamics. [1]

We study here the case of parametric driving, a technique that has been realized in MEMS and NEMS resonators [14,38–40], but parametric excitation is not an essential requirement of our analysis. On the other hand, having weak damping, or a large quality factor, characteristic of typical MEMS and NEMS resonators, is essential for the analysis that follows. First of all, as was demonstrated in a number of earlier examples [41,42], it leads to a clear separation of time scales—a fast scale defined by the high oscillation frequencies of the resonators, and a slow scale defined by the damping rate. This allows us to perform a multiple-scales analysis in Sec. II and obtain amplitude equations to describe the slow dynamics of the system of coupled resonators. It is in the slow dynamics that the homoclinic orbits are found. Secondly, the weak damping, which requires only a weak drive to obtain a response, allows us to treat both the damping and the drive as perturbations, even with respect to the slow dynamics. Therefore, in Sec. III we set the parametric drive amplitude and the damping to zero in the amplitude equations, which makes them integrable. This allows us, in Sec. IV, to find conditions for the existence of homoclinic orbits and to obtain analytical expressions for these orbits. We emphasize that these orbits reside in a four-dimensional phase space, and as such are homoclinic not to a point, but rather to a whole invariant two-dimensional manifold in the shape of a semi-infinite cylinder. Of these, we identify a subset of orbits, satisfying a particular resonance condition, that are precisely heteroclinic, connecting pairs of points in four-dimensional phase space. In Sec. V we reintroduce the drive and the damping into the equations as small perturbations, and use the high-dimensional Melnikov method to determine which of the heteroclinic orbits, determined through the resonance condition in the unperturbed system, survives under the perturbation. In Sec. VI we study the effects of the perturbation on the dynamics within the invariant semi-infinite cylinder near the resonance condition. Finally, in Sec. VII we put everything together by calculating the parameter values for which the end points of the unperturbed heteroclinic orbits are deformed in the perturbed system in such a way that they become connected through the dynamics on the semi-infinite cylinder, producing Šilnikov orbits, homoclinic to a fixed point of a saddle-focus type. We conclude by verifying our analytical calculation using numerical simulations. Our analysis implies that conditions exist in the coupled resonator system that could lead to chaotic motion.

II. NORMAL MODE AMPLITUDE EQUATIONS

We consider a pair of resonators modeled by the equations of motion,

$$\ddot{u}_n + u_n + u_n^3 - \tfrac{1}{2}Q^{-1}(\dot{u}_{n-1} - 2\dot{u}_n + \dot{u}_{n+1}) + \tfrac{1}{2}[D + H\cos\omega_p t](u_{n-1} - 2u_n + u_{n+1}) = 0, \quad (2)$$

for $n = 1,2$, where u_n describes the deviation of the n^{th} resonator from its equilibrium, and we label two fictitious fixed resonators as $u_0 = u_3 = 0$ for convenience. Detailed arguments for the choice of terms introduced into these equations of motion are discussed by Lifshitz and Cross [41], who modeled the particular experimental realization of Buks and Roukes [18], although other variations are possible [12]. The terms include an elastic restoring force as in Eq. (1) with positive linear and cubic contributions (whose coefficients are both scaled to 1), a dc electrostatic nearest-neighbor coupling term with a small ac component responsible for the parametric excitation (with coefficients D and H, respectively), and a linear dissipation term, which is taken to be of a nearest neighbor form, motivated by the experimental indication [18] that most of the dissipation comes from the electrostatic interaction between neighboring beams. Note that the electrostatic attractive force acting between neighboring beams decays with the distance between them, and thus acts to slightly soften the otherwise positive elastic restoring force. Lifshitz and Cross also considered an additional nonlinear damping term, which we neglect here for the sake of simplicity. The resonators' quality factor Q is typically high in MEMS and NEMS devices, which can be used to define a small expansion parameter $\epsilon \ll 1$, by taking $Q^{-1} = \epsilon\hat{\gamma}$, with $\hat{\gamma}$ of order unity. The drive amplitude is then expressed as $H = \epsilon\hat{h}$, in anticipation of the fact that parametric oscillations at half the driving frequency require a driving amplitude which is of the same order as the linear damping rate [12].

Following Appendix B of Lifshitz and Cross [41], we use multiple time scales to express the displacements of the resonators as

$$x_{1,2}(t) = \frac{\sqrt{3\epsilon}}{2}\left(A_1(T)e^{i\omega_1 t} \pm A_2(T)e^{i\omega_2 t} + \text{c.c.}\right) + \epsilon^{3/2}x_{1,2}^{(1)}(t) + \cdots, \quad (3)$$

where x_1 is taken with the positive sign and x_2 with the negative sign; with a slow time $T = \epsilon t$, and where the normal mode frequencies are given by $\omega_1^2 = 1 - D/2$, and $\omega_2^2 = 1 - 3D/2$. Substituting Eq. (3) into the equations of motion (2) generates secular terms that yield two coupled equations for the complex amplitudes $A_{1,2}$. If we measure the drive frequency relative to twice ω_2 by setting $\omega_p = 2\omega_2 + \epsilon\Omega$, express ω_1 relative to ω_2 as $\omega_1 = \omega_2 + 2\epsilon\Omega_1$, and express the complex amplitudes using real amplitudes and phases as

$$A_1(T) = a_1(T)e^{i[\chi_1(T) + (\Omega/2 - 2\Omega_1)T]},$$
$$A_2(T) = a_2(T)e^{i[\chi_2(T) + \Omega T/2]}, \quad (4)$$

the real and imaginary parts of the two secular amplitude equations become

$$\frac{da_1}{dT} = -\frac{1}{4}\hat{\gamma}a_1 - \frac{\hat{h}}{8\omega_1}a_1\sin 2\chi_1 - \frac{9}{8\omega_1}a_2^2 a_1\sin 2(\chi_2 - \chi_1), \quad (5a)$$

$$\frac{d\chi_1}{dT} = 2\Omega_1 - \frac{1}{2}\Omega - \frac{\hat{h}}{8\omega_1}\cos 2\chi_1 + \frac{9}{8\omega_1}\left[a_1^2 + 2a_2^2 + a_2^2\cos 2(\chi_2 - \chi_1)\right], \quad (5b)$$

[1] We should emphasize that the existence of horseshoes does not guarantee the observation of chaos since the orbits created by the horseshoe mechanism are unstable. Nevertheless, merely exposing their presence provides one of the few analytical predictions of chaos.

$$\frac{da_2}{dT} = -\frac{3}{4}\hat{\gamma}a_2 - \frac{3\hat{h}}{8\omega_2}a_2\sin 2\chi_2 - \frac{9}{8\omega_2}a_1^2 a_2 \sin 2(\chi_1-\chi_2), \tag{5c}$$

$$\frac{d\chi_2}{dT} = -\frac{1}{2}\Omega - \frac{3\hat{h}}{8\omega_2}\cos 2\chi_2 + \frac{9}{8\omega_2}\left[a_2^2 + 2a_1^2 + a_1^2\cos 2(\chi_1-\chi_2)\right]. \tag{5d}$$

Steady-state solutions, oscillating at half the parametric drive frequency, are obtained by setting $da_i/dT = d\chi_i/dT = 0$ in Eqs. (5a)–(5d) and solving the resulting algebraic equations. We are interested in extending the investigation of these amplitude equations. In particular, we want to identify the conditions under which they may display chaotic dynamics. We should note that equations similar to (5) were also used for modeling a variety of parametrically driven two-degree-of-freedom systems such as surface waves in nearly square tanks or vibrations of nearly square thin plates or of beams with nearly square cross sections [44–47].

III. UNPERTURBED EQUATIONS—SETTING DAMPING AND DRIVE TO ZERO

We first consider the integrable parts of Eqs. (5a)–(5d), obtained by setting $\hat{\gamma} = \hat{h} = 0$. In Sec. V we will reintroduce the driving and damping terms as a perturbation. We transform the integral part of Eqs. (5a)–(5d) into a more familiar form, which has been studied in the context of higher dimensional Melnikov methods [33,36], by rescaling the amplitudes $a_1 \to a_1\sqrt{\omega_2 8/9}$, and $a_2 \to a_2\sqrt{\omega_1 8/9}$, and changing to two pairs of action-angle variables: (i) $J = a_1^2/2$, $\theta = \chi_1 - \chi_2$; and (ii) $I = (a_1^2 + a_2^2)/2$, $\phi = \chi_2$. After defining $r = \omega_1/\omega_2$, and rescaling time as $T \to T/2$, we obtain the unperturbed Hamilton equations,

$$\frac{dJ}{dT} = -\frac{\partial \tilde{H}_0(J,\theta,I)}{\partial\theta} = 2J(I-J)\sin 2\theta, \tag{6a}$$

$$\frac{d\theta}{dT} = \frac{\partial \tilde{H}_0(J,\theta,I)}{\partial J} = \Omega_1 + I(2-r+\cos 2\theta) - J\left(4 - \frac{r^2+1}{r} + 2\cos 2\theta\right), \tag{6b}$$

$$\frac{dI}{dT} = -\frac{\partial \tilde{H}_0(J,\theta,I)}{\partial\phi} = 0, \tag{6c}$$

$$\frac{d\phi}{dT} = \frac{\partial \tilde{H}_0(J,\theta,I)}{\partial I} = rI - \frac{\Omega}{4} + J(2-r+\cos 2\theta), \tag{6d}$$

where the Hamiltonian $\tilde{H}_0$, which generates these equations, is expressed as

$$\tilde{H}_0(J,\theta,I) = \frac{rI^2}{2} - \frac{\Omega}{4}I - J^2\left(2 - \frac{r^2+1}{2r}\right) + J\left[I(2-r)+\Omega_1\right] + J(I-J)\cos 2\theta. \tag{7}$$

Thus, both I and $\tilde{H}_0$ are constants of the motion in the unperturbed system. Note that $(J,\theta,I,\phi) \in \mathbb{R}^+ \times \mathbb{S} \times \mathbb{R}^+ \times \mathbb{S}$, where $\mathbb{S}$ is the unit circle, and $\mathbb{R}^+$ are the non-negative reals.

It is convenient to describe the dynamics also in terms of the Cartesian variables $x = a_1\cos(\chi_1-\chi_2) = \sqrt{2J}\cos\theta$ and $y = a_1\sin(\chi_1-\chi_2) = \sqrt{2J}\sin\theta$, in place of J and θ, thereby obtaining the Hamilton equations,

$$\frac{dx}{dT} = -\frac{\partial H_0(x,y,I)}{\partial y} = y^3\left(1 - \frac{r^2+1}{2r}\right) + x^2 y\left(2 - \frac{r^2+1}{2r}\right) - y\left[I(1-r)+\Omega_1\right], \tag{8a}$$

$$\frac{dy}{dT} = \frac{\partial H_0(x,y,I)}{\partial x} = -x^3\left(3 - \frac{r^2+1}{2r}\right) - y^2 x\left(2 - \frac{r^2+1}{2r}\right) + x\left[I(3-r)+\Omega_1\right], \tag{8b}$$

$$\frac{dI}{dT} = -\frac{\partial H_0(x,y,I)}{\partial\phi} = 0, \tag{8c}$$

$$\frac{d\phi}{dT} = \frac{\partial H_0(x,y,I)}{\partial I} = rI - \frac{\Omega}{4} + \frac{x^2}{2}(3-r) + \frac{y^2}{2}(1-r), \tag{8d}$$

where y plays the role of a coordinate and x is its conjugate momentum, and where the Hamiltonian H_0 is now given by

$$H_0(x,y,I) = \frac{rI^2}{2} - \frac{\Omega}{4}I - \frac{x^4}{4}\left(3 - \frac{r^2+1}{2r}\right) - \frac{y^4}{4}\left(1 - \frac{r^2+1}{2r}\right) - x^2y^2\left(1 - \frac{r^2+1}{4r}\right) + \frac{x^2}{2}[I(3-r)+\Omega_1] + \frac{y^2}{2}[I(1-r)+\Omega_1]. \tag{9}$$

IV. ANALYTICAL EXPRESSIONS FOR HOMOCLINIC ORBITS

We wish to identify the conditions under which there exist homoclinic orbits in the unperturbed system. These orbits will potentially lead to chaotic dynamics once we reintroduce the damping and the drive in the form of small perturbations. We therefore consider the fixed point $x = y = 0$ in the unperturbed (x,y) plane, as given by Eqs. (8a) and (8b). A linear analysis of this fixed point reveals that it is a saddle for values of the positive constant of motion I, that satisfy the inequality $[I(1-r)+\Omega_1][I(3-r)+\Omega_1] < 0$. This implies that the fixed point at $x = y = 0$ is never a saddle if the fixed parameter $r < 1$; it is a saddle for $1 < r < 3$, if $I > \Omega_1/(r-1)$; and it is a saddle for $r > 3$, if $\Omega_1/(r-1) < I < \Omega_1/(r-3)$. We shall restrict ourselves here to values $1 < r < 3$, therefore to obtain a saddle one must only ensure that $I > \Omega_1/(r-1)$. In the full four-dimensional system given by Eqs. (8a)–(8d) this saddle point describes a two-dimensional invariant semi-infinite cylinder, or annulus,

$$\mathcal{M} = \left\{(x,y,I,\phi)\;\middle|\; x = 0,\ y = 0, \frac{\Omega_1}{r-1} < I\right\}, \quad 1 < r < 3, \tag{10}$$

where ϕ is unrestricted within the unit circle. The trajectories on $\mathcal{M}$ are periodic orbits given by $I =$ constant and $\phi = (rI - \Omega/4)T + \phi_0$. For the resonant value of $I \equiv I^r = \Omega/4r$

the rotation frequency vanishes, and the periodic orbit becomes a circle of fixed points. Of course, this trivial unperturbed dynamics on $\mathscr{M}$ undergoes a dramatic change under the addition of perturbations.

The two-dimensional invariant annulus $\mathscr{M}$ has three-dimensional stable and unstable manifolds, denoted as $W^s(\mathscr{M})$ and $W^u(\mathscr{M})$, respectively, which coincide to form a three-dimensional homoclinic manifold $\Gamma \equiv W^s(\mathscr{M}) \cap W^u(\mathscr{M})$. Trajectories on the homoclinic manifold Γ are homoclinic orbits that connect the origin of the (x,y) plane to itself. Thus, the constant value of the Hamiltonian along such an orbit is equal to its value at the origin, namely $H_0(0,0,I) = H_0(x,y,I) = \tilde{H}_0(J,\theta,I)$, which immediately yields an equation for the homoclinic orbits in terms of the action-angle variables,

$$J^h(\theta,I) = \frac{2r\,[I\,(r-2-\cos 2\theta)-\Omega_1]}{r^2-2r\,(2+\cos 2\theta)+1}. \tag{11}$$

To obtain the temporal dependence of the dynamical variables along the homoclinic orbit, we substitute the homoclinic orbit equation (11) into Eq. (6b), to get

$$\frac{d\theta}{dT} = I(r-2-\cos 2\theta)-\Omega_1. \tag{12}$$

Next, we note that $\chi_1 = \phi + \theta$, and use the Hamiltonian (7) to get

$$\frac{d\chi_1}{dT} = Ir - \frac{\Omega}{4} + J\frac{1-r^2}{2r}. \tag{13}$$

We then integrate Eq. (12), substitute the result into Eq. (11), and the latter into Eq. (13), and finally integrate Eq. (13) to obtain analytical expressions for the temporal dependence of the dynamical variables along orbits that are homoclinic to $\mathscr{M}$.

For $I > 2r\Omega_1/(r^2-1)$ we define $q \equiv I(r^2-1) - 2r\Omega_1 > 0$, and find that $\theta_0 \equiv \theta(T=0) = 0,\pi$, and that the homoclinic orbits are given by

$$J^h(T,I) = \frac{2ra^2}{q\cosh(2aT)+p}, \tag{14a}$$

$$\tan(\theta^h(T,I)) = -\sqrt{\frac{I(r-3)-\Omega_1}{I(1-r)+\Omega_1}}\tanh(aT), \tag{14b}$$

$$\chi_1^h(T,I) = -\frac{a(r^2-1)}{\sqrt{p^2-q^2}}\operatorname{arctanh}\left(\sqrt{\frac{p-q}{p+q}}\tanh aT\right) + \left(rI-\frac{\Omega}{4}\right)T + \chi_1(0), \tag{14c}$$

$$\phi^h(T,I) = \chi_1^h(T,I) - \theta^h(T,I), \tag{14d}$$

where

$$\begin{aligned} p &= \Omega_1(r^2-4r+1) - I(r^3-6r^2+7r-2), \\ a^2 &= -\Omega_1^2 + 2I\Omega_1(r-2) - I^2(r-3)(r-1). \end{aligned} \tag{15}$$

For $I < 2r\Omega_1/(r^2-1)$ we redefine $q \equiv 2r\Omega_1 - I(r^2-1) > 0$, and find that $\theta_0 = \pm\pi/2$, and that the homoclinic orbits are given by Eqs. (14a)–(14d), with

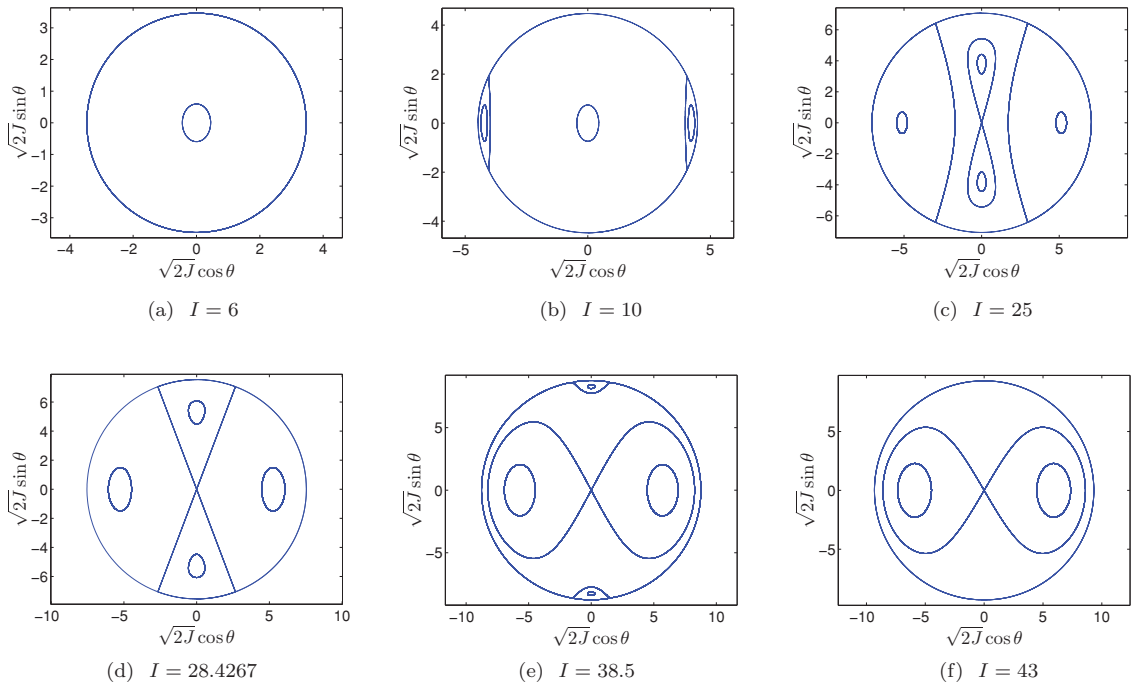

(a) $I = 6$ (b) $I = 10$ (c) $I = 25$

(d) $I = 28.4267$ (e) $I = 38.5$ (f) $I = 43$

FIG. 1. (Color online) Numerical phase portraits of the unperturbed (x,y) plane for $r = 2$, $\Omega_1 = 21.32$, and different values of I as noted in the individual captions. All figures show the trajectories for which J has a fixed value equal to I. As explained in the text and for $r = 2$, four hyperbolic fixed points appear on the $J = I$ circle for $2\Omega_1/5 = 8.528 < I < 2\Omega_1 = 42.64$; the $J = 0$ fixed point changes from a center to a saddle at $I = \Omega_1 = 21.32$; and a global bifurcation rotating the homoclinic orbit through an angle of $\pi/2$, shown in panel (d), occurs at $I = 4\Omega_1/3 \simeq 28.42$.

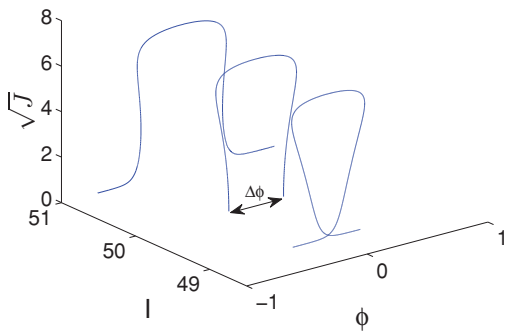

FIG. 2. (Color online) Orbits homoclinic to $\mathscr{M}$. For $I = I^r$ (the orbit in the middle), $d\phi/dT = 0$ on $\mathscr{M}$, and the orbit is heteroclinic, connecting fixed points on $\mathscr{M}$ that are $\Delta\phi$ apart. For $I \lesseqgtr I^r$, $d\phi/dT \gtreqless 0$ on $\mathscr{M}$. The parameters are $r = 2, \Omega = 400, \Omega_1 = 21.32$.

Eq. (14b) replaced by

$$\cot(\theta^h(T,I)) = -\sqrt{\frac{I(1-r)+\Omega_1}{I(r-3)-\Omega_1}}\tanh(aT). \tag{16}$$

Thus, exactly at $I = 2r\Omega_1/(r^2-1)$, or $q = 0$, there is a global bifurcation in which the homoclinic orbit rotates through an angle of $\pi/2$.

Some of the phase-space portraits of the unperturbed (x,y) plane are calculated numerically from Eqs. (6a) and (6b), for different values of I, and shown in Fig. 1. From Eq. (6a) it follows that the value of J is fixed if (a) $J = 0$; or (b) $J = I$; or (c) θ is an integer multiple of $\pi/2$ and θ is fixed. Figures 1(a)–1(f) all show the trajectories for which J has a fixed value equal to I. Four hyperbolic fixed points appear on the $J = I$ circle for $\Omega_1/(3-1/r) \leqslant I \leqslant \Omega_1(1-1/r)$, where solutions exist to the equation $\partial\theta/\partial T = 0$ with J replaced by I [Figs. 1(b)–1(e)]. As expected, the origin $J = 0$ is always a fixed point—a center for small values of I [Figs. 1(a) and 1(b)], which undergoes a pitchfork bifurcation into a saddle when $\partial\theta/\partial T = 0$ with $J = 0$, occurring at $I = \Omega_1/(r-1)$ [Figs. 1(c)–1(f)]. Additional centers appear whenever θ is an integer multiple of $\pi/2$ and solutions exist to the equation $\partial\theta/\partial T = 0$ with $\cos 2\theta = \pm 1$ [Figs. 1(b)–1(f)]. The global bifurcation at $I = 2\Omega_1 r/(r^2-1)$ where the homoclinic orbit rotates by $\pi/2$ is shown in Fig. 1(d).

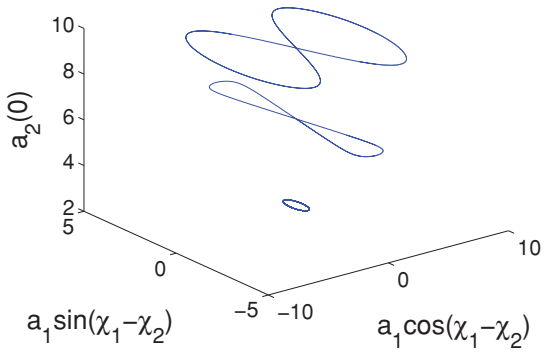

FIG. 3. (Color online) Results of a numerical integration of Eqs. (5a)–(5d) for different values of the initial amplitude of the second mode $a_2(0)$, with $\hat{h} = \hat{\gamma} = 0$, $\omega_1 = 0.8528$, $\omega_2 = \omega_1/2$, $\Omega_1 = 21.32$, and $\Omega = 400$. As expected, for $a_2(0) > \sqrt{16\Omega_1\omega_1\omega_2/9(\omega_1-\omega_2)} \simeq 5.68$ the origin becomes a saddle, which rotates through an angle of $\pi/2$ at $a_2(0) = \sqrt{32\Omega_1\omega_1^2\omega_2/9(\omega_1^2-\omega_2^2)} \simeq 6.46$.

Note that we refer to the orbits given by Eqs. (14a)–(14d) as homoclinic since they are homoclinic to $\mathscr{M}$. A few of these orbits are shown in Fig. 2. At resonance, for $I = I^r$, the orbits are truly heteroclinic, connecting fixed points that are $\Delta\phi$ apart, where $\Delta\phi = \Delta\chi_1 - \Delta\theta$, and

$$\Delta\theta = -2\arctan\sqrt{\frac{I^r(r-3)-\Omega_1}{I^r(1-r)+\Omega_1}}, \tag{17a}$$

$$\Delta\chi_1 = -\frac{2a(r^2-1)}{\sqrt{p^2-q^2}}\operatorname{arctanh}\sqrt{\frac{p-q}{p+q}}, \tag{17b}$$

and where for any variable f, $\Delta f \equiv f(\infty) - f(-\infty)$. Such an unperturbed heteroclinic orbit is shown in the middle of Fig. 2.

We wish to demonstrate the results obtained so far also in terms of the original amplitude equations [Eqs. (5a)–(5d)] with $\hat{h} = \hat{\gamma} = 0$. The point $x = y = 0$ corresponds to $a_1 = 0$ in Eqs. (5a)–(5d). To start the simulation near this point, we initiate the numerical solution with $a_1(0) \ll 1$, which through the definition of I implies that $a_2(0) \simeq \sqrt{16I\omega_1/9}$. The condition for having a saddle at the origin of Eqs. (8a) and (8b), $I > \Omega_1/(r-1)$, translates into the condition $a_2(0) > \sqrt{16\Omega_1\omega_1/9(r-1)} = \sqrt{16\Omega_1\omega_1\omega_2/9(\omega_1-\omega_2)}$. The condition for the global bifurcation, rotating the homoclinic orbit through $\pi/2$, given by $I = 2r\Omega_1/(r^2-1)$, translates into $a_2(0) = \sqrt{32\Omega_1\omega_1^2\omega_2/9(\omega_1^2-\omega_2^2)}$. These conditions are verified by a numerical integration of Eqs. (5a)–(5d) by varying the initial amplitude of the out-of-phase mode, $a_2(0)$, as shown in Fig. 3.

V. HOMOCLINIC INTERSECTIONS IN THE PERTURBED SYSTEM

After having calculated the homoclinic orbits in the unperturbed system, we now reintroduce the drive and the damping as perturbations and study how they affect the dynamics. In particular, we want to study the nature of the invariant annulus $\mathscr{M}$, and its stable and unstable manifolds, $W^s(\mathscr{M})$ and $W^u(\mathscr{M})$, under the perturbation, and use the Melnikov criterion to find the conditions under which they can still intersect. It is instructive to write the perturbed system in terms of the action-angle variables in the general form,

$$\frac{dJ}{dT} = -\frac{\partial\tilde{H}_0(J,\theta,I)}{\partial\theta} + \xi g^J = -\frac{\partial\tilde{H}_0(J,\theta,I)}{\partial\theta} + \xi\left(-\frac{\partial\tilde{H}_1(J,\theta,I,\phi)}{\partial\theta} + d^J\right), \tag{18a}$$

$$\frac{d\theta}{dT} = \frac{\partial\tilde{H}_0(J,\theta,I)}{\partial J} + \xi g^\theta = \frac{\partial\tilde{H}_0(J,\theta,I)}{\partial J} + \xi\frac{\partial\tilde{H}_1(J,\theta,I,\phi)}{\partial J}, \tag{18b}$$

$$\frac{dI}{dT} = \xi g^I = \xi\left(-\frac{\partial \tilde{H}_1(J,\theta,I,\phi)}{\partial\phi} + d^I\right), \tag{18c}$$

$$\frac{d\phi}{dT} = \frac{\partial \tilde{H}_0(J,\theta,I)}{\partial I} + \xi g^\phi = \frac{\partial \tilde{H}_0(J,\theta,I)}{\partial I} + \xi\frac{\partial \tilde{H}_1(J,\theta,I,\phi)}{\partial I}, \tag{18d}$$

where we have quantified the perturbations by expressing the drive amplitude and the damping as $\hat{h} = 8\xi\omega_1 h$ and $\hat{\gamma} = 4\xi\gamma$, respectively, where $\xi \ll 1$ is a small parameter. The perturbations due to the parametric drive are generated from the Hamiltonian,

$$\tilde{H}_1(J,\theta,I,\phi) = -\frac{h}{2}\left[J\cos 2(\phi+\theta) + 3r(I-J)\cos 2\phi\right], \tag{19}$$

and the dissipative perturbations are given by $d^J = -\gamma J$ and $d^I = -\gamma(3I - 2J)$. Similarly, in terms of the Cartesian variables, the perturbed system is written in this general form as

$$\frac{dx}{dT} = -\frac{\partial H_0(x,y,I)}{\partial y} + \xi g^x = -\frac{\partial H_0(x,y,I)}{\partial y} + \xi\left(-\frac{\partial H_1(x,y,I,\phi)}{\partial y} + d^x\right), \tag{20a}$$

$$\frac{dy}{dT} = \frac{\partial H_0(x,y,I)}{\partial x} + \xi g^y = \frac{\partial H_0(x,y,I)}{\partial x} + \xi\left(\frac{\partial H_1(x,y,I,\phi)}{\partial x} + d^y\right), \tag{20b}$$

$$\frac{dI}{dT} = \xi g^I = \xi\left(-\frac{\partial H_1(x,y,I,\phi)}{\partial\phi} + d^I\right), \tag{20c}$$

$$\frac{d\phi}{dT} = \frac{\partial H_0(x,y,I)}{\partial I} + \xi g^\phi = \frac{\partial H_0(x,y,I)}{\partial I} + \xi\frac{\partial H_1(x,y,I,\phi)}{\partial I}, \tag{20d}$$

with

$$H_1(x,y,I,\phi) = \frac{h}{4}\{[(3r-1)x^2 + (3r+1)y^2 - 6rI]\cos 2\phi + 2xy\sin 2\phi\}, \tag{21}$$

and where $d^x = -\gamma x/2$, $d^y = -\gamma y/2$, and $d^I = -\gamma(3I - x^2 - y^2)$.

For $0 < \xi \ll 1$ the unperturbed invariant annulus $\mathscr{M}$, and its stable and unstable manifolds, $W^s(\mathscr{M})$ and $W^u(\mathscr{M})$, persist as a *locally invariant* annulus $\mathscr{M}_\xi$ with stable and unstable manifolds, $W^s(\mathscr{M}_\xi)$ and $W^u(\mathscr{M}_\xi)$ [33,36,44,47]. Due to the fact that we use parametric rather than direct excitation, the point $x = y = 0$ remains a fixed point of the perturbed Eqs. (20a) and (20b), so $\mathscr{M}_\xi$ is defined just like $\mathscr{M}$ in Eq. (10). However, the term *locally invariant* means that trajectories with initial conditions on $\mathscr{M}_\xi$ may leave it through its lower boundary at $I = \Omega_1/(r-1)$. We want to find intersections of the manifolds $W^s(\mathscr{M}_\xi)$ and $W^u(\mathscr{M}_\xi)$, because such intersections may contain orbits that are homoclinic to $\mathscr{M}_\xi$. This is done by calculating the Melnikov integral, $M(I,\phi_0)$, which is a measure of the distance between these manifolds. If the Melnikov integral has simple zeros [$M(I,\phi_0) = 0$ and $\partial M(I,\phi_0)/\partial\phi_0 \neq 0$], the three-dimensional manifolds $W^s(\mathscr{M}_\xi)$ and $W^u(\mathscr{M}_\xi)$ intersect transversely along two-dimensional surfaces.

The Melnikov integral is given by [33,36]

$$M(I,\phi_0) = \int_{-\infty}^{\infty}\langle \mathbf{n}(x^h,y^h,I), \mathbf{g}(x^h,y^h,I,\phi^h+\phi_0)\rangle dT, \tag{22}$$

where

$$\mathbf{n}(x,y,I) = \left(\frac{\partial H_0(x,y,I)}{\partial x}, \frac{\partial H_0(x,y,I)}{\partial y}, \frac{\partial H_0(x,y,I)}{\partial I} - \frac{\partial H_0(0,0,I)}{\partial I}\right), \tag{23}$$

$$\mathbf{g}(x,y,I,\phi) = (g^x, g^y, g^I), \tag{24}$$

$x^h(T,I)$, $y^h(T,I)$, and $\phi^h(T,I)$ are the homoclinic orbits given by Eqs. (14a)–(14d), and angular brackets denote the standard inner product. At resonance, the Melnikov integral $M(I^r,\phi_0)$ can be calculated explicitly, because then $\partial H_0(0,0,I^r)/\partial I = 0$ and the integrand of the Melnikov integral is given by

$$\begin{aligned}\langle \mathbf{n},\mathbf{g}\rangle &= \frac{\partial H_0}{\partial x}g^x + \frac{\partial H_0}{\partial y}g^y + \frac{\partial H_0}{\partial I}g^I \\ &= -\frac{\partial H_0}{\partial x}\frac{\partial H_1}{\partial y} + \frac{\partial H_0}{\partial y}\frac{\partial H_1}{\partial x} - \frac{\partial H_0}{\partial I}\frac{\partial H_1}{\partial\phi} \\ &\quad + \frac{\partial H_0}{\partial x}d^x + \frac{\partial H_0}{\partial y}d^y + \frac{\partial H_0}{\partial I}d^I.\end{aligned} \tag{25}$$

For the unperturbed orbits we can use the chain rule and the fact that $dI/dT = 0$ to obtain the relation,

$$\frac{dH_1}{dT} = \frac{\partial H_0}{\partial x}\frac{\partial H_1}{\partial y} - \frac{\partial H_0}{\partial y}\frac{\partial H_1}{\partial x} + \frac{\partial H_0}{\partial I}\frac{\partial H_1}{\partial\phi}, \tag{26}$$

so the Melnikov integrand reduces to

$$\langle \mathbf{n},\mathbf{g}\rangle = -\frac{dH_1}{dT} + \frac{\partial H_0}{\partial x}d^x + \frac{\partial H_0}{\partial y}d^y + \frac{\partial H_0}{\partial I}d^I. \tag{27}$$

Upon transforming to the action-angle variables one has

$$\frac{\partial H_0}{\partial x}d^x + \frac{\partial H_0}{\partial y}d^y = \frac{\partial \tilde{H}_0}{\partial J}d^J, \tag{28}$$

and so the integrand (27) becomes

$$\begin{aligned}\langle \mathbf{n},\mathbf{g}\rangle &= -\frac{d\tilde{H}_1}{dT} + \frac{\partial \tilde{H}_0}{\partial J}d^J + \frac{\partial \tilde{H}_0}{\partial I}d^I \\ &= -\frac{d\tilde{H}_1}{dT} - \gamma J\frac{d\theta}{dT} - \gamma(3I^r - 2J)\frac{d\phi}{dT} \\ &= -\frac{d\tilde{H}_1}{dT} - 3\gamma I^r\frac{d\phi}{dT} + 2\gamma J\frac{d\chi_1}{dT} - 3\gamma J\frac{d\theta}{dT},\end{aligned} \tag{29}$$

where we recall that $\chi_1 = \theta + \phi$. We explicitly integrate each of the terms in the integrand (29) in Appendix A, and find that

$$M(I^r,\phi_0) = -3rI^r h\sin 2\phi_0\sin\Delta\phi - \gamma(3I^r\Delta\chi_1 + 3\Delta\mu - 2\Delta\sigma), \tag{30}$$

where $\Delta\sigma$ and $\Delta\mu$ are defined in Eqs. (A2) and (A4), respectively. Except for the special case in which the phase difference $\Delta\phi$ is a multiple of π, the function $M(I^r,\phi_0)$ has simple zeros as long as the relation,

$$\left|\frac{\gamma(3I^r\Delta\chi_1 + 3\Delta\mu - 2\Delta\sigma)}{3rI^r h\sin\Delta\phi}\right| < 1, \tag{31}$$

is satisfied. If the system parameters satisfy this condition, every simple zero of the Melnikov function corresponds to two symmetric (due to the invariance $x,y \to -x,-y$) two-dimensional intersection surfaces. The $\xi \to 0$ limit of these surfaces contains orbits whose explicit form is given by Eqs. (14a)–(14d) with their I and ϕ_0 values satisfying the relation $M(I,\phi_0) = 0$, for I close to I^r [36]. Thus, an unperturbed heteroclinic orbit given by Eqs. (14a)–(14d), with $I = I^r$ and a phase ϕ_0 at time zero, can be made to persist under the perturbation by setting the drive amplitude to the value,

$$h = \frac{\gamma(2\Delta\sigma - 3I^r\Delta\chi_1 - 3\Delta\mu)}{3rI^r \sin 2\phi_0 \sin\Delta\phi}. \tag{32}$$

We give numerical evidence of this in Sec. VII. Such orbits surviving in the intersection of $W^u(\mathcal{M}_\xi)$ and $W^s(\mathcal{M}_\xi)$ may leave the stable manifold $W^s(\mathcal{M}_\xi)$ in forward time, and the unstable manifold $W^u(\mathcal{M}_\xi)$ in backward time, through the low boundary at $I = \Omega_1/(r-1)$, since these manifolds are only locally invariant [36]. However, the analysis we perform below allows us to find surviving homoclinic orbits that are contained in the intersection of $W^u(\mathcal{M}_\xi)$ and $W^s(\mathcal{M}_\xi)$.

VI. DYNAMICS NEAR RESONANCE

After having calculated the Melnikov integral at $I = I^r$, we proceed to examine the dynamics on $\mathcal{M}_\xi$ near this resonance. The equations that describe the dynamics on $\mathcal{M}_\xi$ are obtained by setting $J = 0$ in Eqs. (18c) and (18d),

$$\frac{dI}{dT} = -\xi 3I(hr\sin 2\phi + \gamma), \tag{33a}$$

$$\frac{d\phi}{dT} = -\frac{\Omega}{4} + rI - \xi\frac{3hr}{2}\cos 2\phi. \tag{33b}$$

To investigate the slow dynamics, which is induced by the perturbation on $\mathcal{M}_\xi$ near resonance, we follow Kovačič and Wiggins [36] and introduce a slow variable $I = I^r + \sqrt{\xi}\rho$ into Eqs. (33a) and (33b), along with a slow time scale $\tau = \sqrt{\xi}T$, and obtain

$$\frac{d\rho}{d\tau} = -3(I^r + \sqrt{\xi}\rho)(hr\sin 2\phi + \gamma), \tag{34a}$$

$$\frac{d\phi}{d\tau} = r\rho - \sqrt{\xi}\frac{3hr}{2}\cos 2\phi. \tag{34b}$$

The leading terms in Eqs. (34a) and (34b), independent of ξ, yield

$$\frac{d\rho}{d\tau} = -3I^r(hr\sin(2\phi) + \gamma) = -\frac{\partial\mathcal{H}(\rho,\phi)}{\partial\phi}, \tag{35a}$$

$$\frac{d\phi}{d\tau} = r\rho = \frac{\partial\mathcal{H}(\rho,\phi)}{\partial\rho}, \tag{35b}$$

where

$$\mathcal{H}(\rho,\phi) = \tfrac{1}{2}r\rho^2 - \tfrac{3}{2}hrI^r\cos(2\phi) + 3\gamma I^r\phi \tag{36}$$

is a rescaled effective Hamiltonian that governs the slow dynamics on $\mathcal{M}_\xi$ close to resonance.

Figure 4(a) shows the phase portrait of Eqs. (35a) and (35b), which contains a saddle q_0 at $(\rho = 0, \phi = \phi_s = [\arcsin b - \pi]/2)$, and a center p_0 at $(\rho = 0, \phi = \phi_c = -[\arcsin b]/2)$, where $b \equiv \gamma/hr$. The fixed points of Eqs. (34a) and (34b) that contain the additional $O(\sqrt{\xi})$ terms are $q_\xi = (-\rho_\xi, \phi_s)$ and $p_\xi = (\rho_\xi, \phi_c)$, where $\rho_\xi = \sqrt{\xi}3h\sqrt{1-b^2}/2$. For small positive ξ, a linear analysis of these fixed points reveals that q_ξ is still a saddle but that p_ξ is a sink, as shown in Fig. 4(b). The fixed points of the full equations (33) near $I = I^r$ are the same saddle and sink, located at $(I = I^-, \phi = \phi_s)$ and $(I = I^+, \phi = \phi_c)$, respectively, where $I^\pm = I^r \pm \sqrt{\xi}\rho_\xi$.[2]

[2]In the full four-dimensional system given by Eqs. (20a)–(20d), the saddle-focus fixed point $(x = 0, y = 0, I = I^+, \phi = \phi_c)$ and saddle fixed point $(x = 0, y = 0, I = I^-, \phi = \phi_s)$ correspond to unstable single-mode oscillations of the antisymmetric mode (that has the smaller linear frequency ω_2). This is also true in the integrable limit ($\xi = 0$), however in this case the eigenvalues describing the

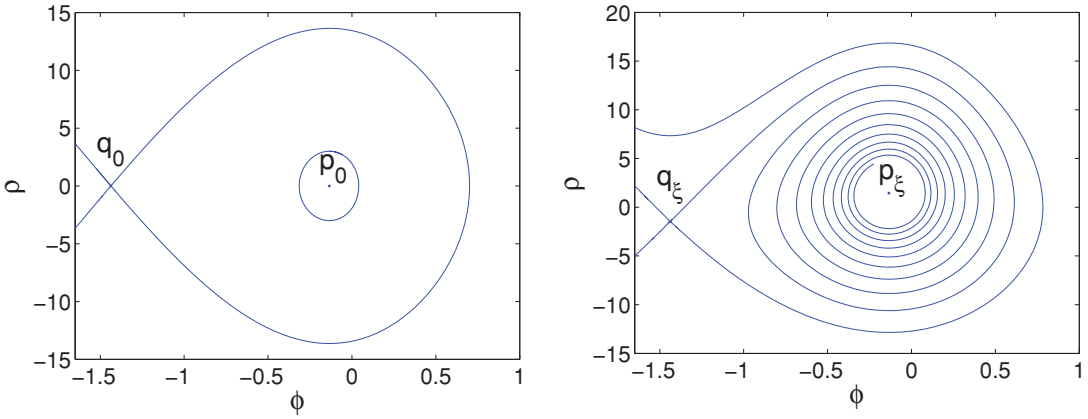

(a) $\xi = 0$ (b) $\xi = 1$

FIG. 4. (Color online) (a) Numerical phase portraits of Eqs. (34a) and (34b) with $\xi = 0$ [or equivalently, Eqs. (35a) and (35b)], showing a saddle and a center. (b) Numerical phase portraits of Eqs. (34a) and (34b) with $\xi = 1$, showing that the saddle remains a saddle but that the center becomes a sink, with their ρ coordinates shifted slightly down and up, respectively. The parameters are $r = 2, \Omega = 400, h = 1, b = 0.2649, \gamma = hbr$.

The scaled equations (35) provide an estimate for the basin of attraction of the sink, which is the area confined within the homoclinic orbit connecting the saddle q_0 to itself, shown in Fig. 4(a). Recall that the dynamics on the unperturbed annulus $\mathscr{M}$ is composed of simple one-dimensional flows, which on resonance turn into a circle of fixed points. Upon adding the small perturbation, two of these fixed points persist in an interval of length π, and the phase space contains two-dimensional flows. Of particular interest is the basin of attraction of the sink, because a homoclinic orbit to a fixed point of this type offers a mechanism for producing chaotic motion. This mechanism, which results from the existence of a homoclinic trajectory to a saddle-focus fixed point, was described by Šilnikov [37]. Obtaining an estimate for the basin of attraction of the sink, allows us to pick out the trajectories satisfying Šilnikov's theorem, which we do in the following section.

VII. A HOMOCLINIC CONNECTION TO THE SINK p_ξ

We are finally in a position to show the existence of an orbit homoclinic to the sink p_ξ.[3] To achieve this, we first show that there exists a homoclinic orbit that approaches p_ξ asymptotically backward in time, and approaches the perturbed annulus $\mathscr{M}_\xi$ asymptotically forward in time. We then estimate the conditions under which the perturbed counterpart of the point, which is reached on $\mathscr{M}$ forward in time in the unperturbed system, lies within the basin of attraction of the sink p_ξ on $\mathscr{M}_\xi$. This gives us an estimate for the possibility of obtaining a Šilnikov orbit that connects the sink back to itself.

The first step is done by finding the conditions for which the Melnikov function $M(I^r,\phi_0=\phi_c+\Delta\phi/2)$ has simple zeros. We substitute $\phi_0=\phi_c+\Delta\phi/2$ into the first term in Eq. (30), and recall that $\sin 2\phi_c=-b$, to get

$$\sin 2\phi_0 \sin\Delta\phi = \tfrac{1}{2}\left[\sqrt{1-b^2}(1-\cos 2\Delta\phi) - b\sin 2\Delta\phi\right]. \tag{37}$$

By substituting (37) into the Melnikov function (30) and equating it to zero we obtain the equation,

$$\begin{aligned} &3I^r\left[\sqrt{1-b^2}(1-\cos 2\Delta\phi) - b\sin 2\Delta\phi\right] \\ &\quad + 2b(3I^r\Delta\chi_1 + 3\Delta\mu - 2\Delta\sigma) = 0, \end{aligned} \tag{38}$$

from which we extract an explicit expression for the condition on b, ensuring the existence of an orbit that asymptotes to p_ξ backward in time, and to $\mathscr{M}_\xi$ forward in time,

$$|b| = \frac{1-\cos 2\Delta\phi}{\sqrt{\left(\frac{4}{3I^r}\Delta\sigma + \sin 2\Delta\phi - 2\Delta\chi_1 - \frac{2\Delta\mu}{I^r}\right)^2 + (1-\cos 2\Delta\phi)^2}}. \tag{39}$$

flow in directions tangent to $\mathscr{M}_\xi$ vanish, so the corresponding fixed points $(x=0,y=0,I=I^r,\phi=\phi_c,\phi_s)$ are saddles, with the nearby linearized vector field described by a pair of real eigenvalues (one positive and one negative) and a pair of zero eigenvalues.

[3]Note that for a particular set of parameters the existence of such an orbit implies the existence of another symmetric orbit due to the invariance $(x,y)\to(-x,-y)$.

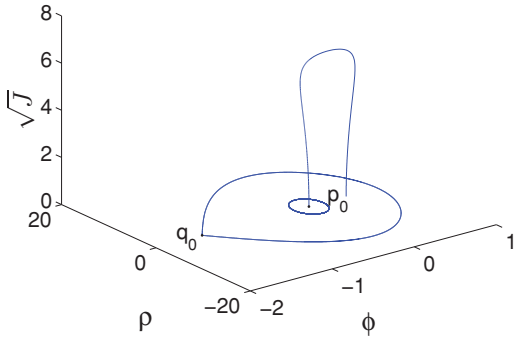

FIG. 5. (Color online) The heteroclinic orbit given by Eqs. (14a)–(14d) with $I=I^r$, superimposed with the phase portrait of the unperturbed scaled system on $\mathscr{M}_\xi$ near resonance, given by Eqs. (35a) and (35b). The parameters are the same as in Fig. 4(a), with $\Omega_1=21.32$. For these parameters $b=0.2949$ according to Eq. (39), so we fix $h=1$ and $\gamma=rbh$ in Eqs. (35a) and (35b). This value of b sets $\phi(-\infty)=\phi_c=-0.1341$, and as can be seen from the figure $\phi_s<\phi(\infty)=\phi_c+\Delta\phi<\phi_m$.

Next, we wish to find an approximate condition, ensuring that this orbit approaches p_ξ as $T\to\infty$. To do so we find the condition for which the *unperturbed* heteroclinic orbit, which asymptotes to p_0 as $T\to-\infty$, returns back to a point on the circle of fixed points that is inside the homoclinic separatrix loop connecting the saddle q_0 to itself [36]. Such an orbit is shown in Fig. 5. This condition is formulated in terms of the difference $\Delta\phi$ between the asymptotic values of the angular variable ϕ as

$$\phi_s<\phi_c+\Delta\phi<\phi_m, \tag{40}$$

where ϕ_m is the maximal value of ϕ on the homoclinic orbit, connecting the saddle q_0 to itself. Since the Hamiltonian (36) is conserved along an orbit, ϕ_m satisfies the equation,

$$\begin{aligned} 0=\mathscr{H}(0,\phi_m)-\mathscr{H}(0,\phi_s) = 3I^r hr\Bigg[&\frac{1}{2}\sqrt{1-b^2}+\frac{1}{2}\cos 2\phi_m \\ &- b\left(\phi_m+\frac{\pi}{2}-\frac{1}{2}\arcsin b\right)\Bigg], \end{aligned} \tag{41}$$

whose roots are found numerically to obtain ϕ_m.

Equations (39) and (40) define conditions for the existence of orbits homoclinic to the sink p_ξ. We wish to relate these results to the actual physical parameters of the coupled resonators. Recall that r sets the value of the electrostatic coupling coefficient $D=2(r^2-1)/(3r^2-1)$. The scaled frequency Ω_1 is then given by $\Omega_1=(\omega_1-\omega_2)/2\epsilon=(\sqrt{1-D/2}-\sqrt{1-3D/2})/2\epsilon$, so after fixing ϵ it is also determined by r. The ratio $b=\gamma/hr$, between the damping coefficient and the drive amplitude, has to be positive in order for the damping coefficient γ to be positive and have the standard physical meaning of energy dissipation. The ratio b is positive if the inequality,

$$\frac{4}{3I^r}\Delta\sigma+\sin 2\Delta\phi-2\Delta\chi_1-\frac{2\Delta\mu}{I^r}>0, \tag{42}$$

is satisfied. We plot the left-hand side of this inequality as a function of Ω and r in Fig. 6(a), and find that for the chosen

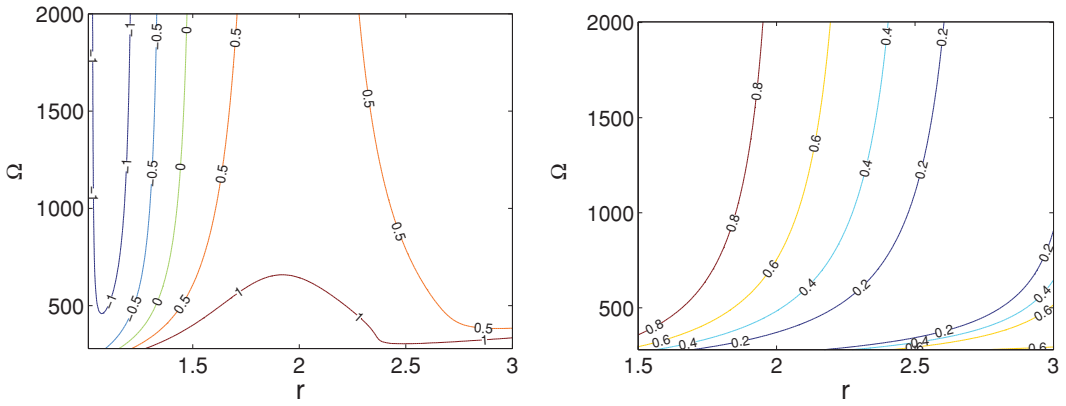

FIG. 6. (Color online) (a) Contour plot of the left-hand side of the inequality (42). In the displayed range of Ω, for $r \gtrsim 1.5$, this function is positive and the coefficient γ represents energy dissipation. For fixed $\epsilon = 0.01$ and $1 < r < 3$, the scaled frequency Ω_1 reaches values of $0 < \Omega_1 < 28$. (b) The ratio $b = \gamma/hr$, given by Eq. (39), as a function of Ω and r ($\epsilon = 0.01$). Here $1.5 < r < 3$ and b is positive.

parameters it is positive if $r \gtrsim 1.5$. Consequently we plot the ratio b in Fig. 6(b) for $1.5 < r < 3$. This value of b then determines the ϕ values of the fixed points of Eq. (35), which are shown in Fig. 7(a), along with $\phi_c + \Delta\phi$ and ϕ_m for a particular value of Ω. The parameter values for which these ϕ values satisfy the condition (40) are displayed in Fig. 7(b), which outlines the values of the electrostatic coupling and parametric driving frequency, for which orbits homoclinic to the sink p_ξ exist. We note that Šilnikov orbits were also found in other two-mode parametrically driven systems [44,45,48], however, slightly different equations were studied, resulting in different phase space dynamics for the unperturbed system as well as different perturbations.

Finally, we wish to verify our calculations by a numerical solution of the ordinary differential equations (ODEs) (18). The difficulty in producing a Šilnikov orbit in these equations is that the linearized growth rates of the saddle-focus fixed point—a saddle on the (J,θ) plane and a focus on the perturbed annulus $\mathscr{M}_\xi$—are $O(\xi)$ in directions tangent to $\mathscr{M}_\xi$, so the orbit has to spend a lot of time near $\mathscr{M}_\xi$ in order to spiral around the saddle focus. However, the linearized growth rates of this fixed point in directions transverse to $\mathscr{M}_\xi$, are $O(1)$, so a small and inevitable numerical error would deflect the orbit away from $\mathscr{M}_\xi$. To avoid this problem we solve the ODEs (18) using a cutoff criterion. We initiate the numerical solution with $J \ll 1$, and the exact coordinates of the sink on $\mathscr{M}_\xi$, $(I = I^+, \phi = \phi_c)$. The orbit initially flows away from $\mathscr{M}_\xi$ and later turns around and approaches it. If on its way back toward $\mathscr{M}_\xi$, the orbit approaches it close enough to satisfy $J < \xi/1000$, we set $dJ/dT = d\theta/dT = 0$ in Eq. (18), thus restricting the motion to be tangent to $\mathscr{M}_\xi$. This numerical scheme allows us to verify our predictions, because as shown in Fig. 8, only when the damping coefficient is equal to $\gamma = hbr$ ($\pm \sim 0.1\%$), with b given by Eq. (39), is our cutoff criterion for eliminating the motion transverse to $\mathscr{M}_\xi$ satisfied. Furthermore, Figs. 8(a) and 8(d), demonstrate that in order to obtain a Šilnikov orbit, the condition (40) needs to be satisfied as well.

Owing to a theorem of Šilnikov [36], the existence of orbits homoclinic to a saddle-focus fixed point in Eq. (18) implies

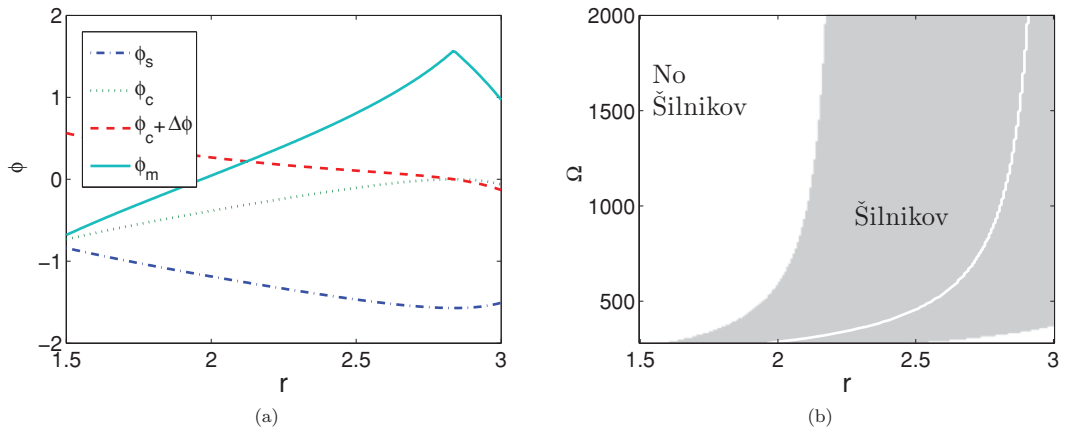

FIG. 7. (Color online) (a) The values of ϕ_s, ϕ_c, $\phi_c + \Delta\phi$, and ϕ_m as functions of r, for $\Omega = 1135.64$. For $r > 2.12$ the condition (40) is satisfied and orbits homoclinic to the sink p_ξ exists, except when $\Delta\phi = 0$. (b) Parameter values for which the condition (40) is satisfied are indicated in gray. The white line inside the gray area corresponds to $\Delta\phi = 0$, where the theory does not apply. In both figures $\epsilon = 0.01$.

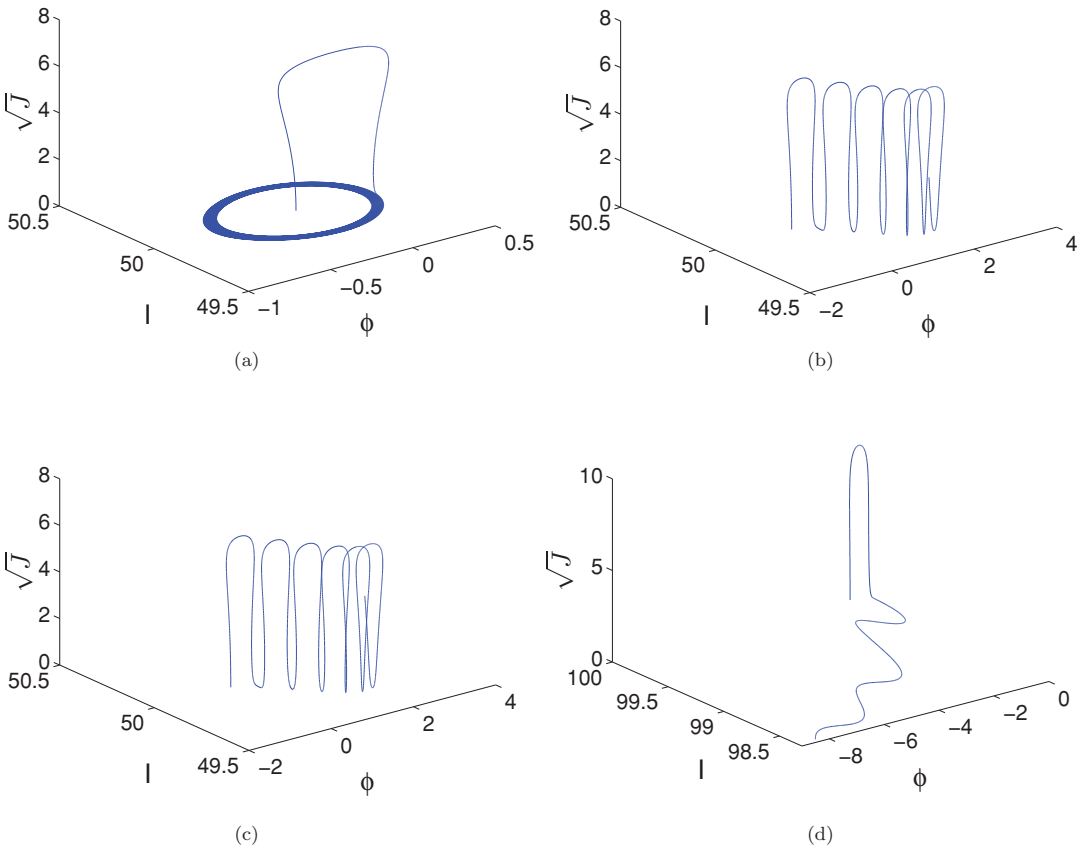

FIG. 8. (Color online) Results of our numerical scheme for $\xi = 0.001$ and the rest of the parameters as in Fig. 5. (a) An illustration of the Šilnikov orbit that is obtained for $\gamma = hbr$ (The $\xi \to 0$ limit of this orbit is shown in Fig. 5.) For (b) $\gamma = h(b - 0.0003)r$, and (c) $\gamma = h(b + 0.0002)r$, and we see that the orbit does not get close enough to $\mathscr{M}_\xi$ in order to meet our cutoff criterion for being homoclinic to it. (d) For $\Omega = 800$, we obtain an orbit that approaches $\mathscr{M}_\xi$ by setting the appropriate value of γ ($b = 0.6178$), however, this orbit does not asymptote to the saddle focus, in agreement with Fig. 7(b). In this simulation, the orbit leaves $\mathscr{M}_\xi$ through its boundary at $I = \Omega_1/(r - 1)$ and eventually $I \to 0$ and the motion dies out.

that these equations contain chaotic motion in the sense of horseshoes in their dynamics.[4]

VIII. SUMMARY

We have studied the origin of chaotic dynamics, and provided conditions for its existence, in a case of two parametrically driven nonlinear resonators. This was achieved by applying a method of Kovačič and Wiggins on transformed amplitude equations that were derived from the equations of motion, which model an actual experimental realization of coupled nanomechanical resonators. We considered the amplitude of the drive and the damping to be small perturbations and obtained explicit expressions for orbits homoclinic to a two-dimensional invariant annulus in the unperturbed equations. At resonance, we were able to calculate the Melnikov integral analytically, and to provide a primary condition for having homoclinic orbits in the full, perturbed equations. By further studying the effects of perturbations on the invariant annulus near resonance, we found a secondary condition for the existence of orbits homoclinic to a fixed point of a saddle-focus type. We used a numerical scheme to verify our theoretical predictions. Such Šilnikov homoclinic orbits give rise to a particular type of horseshoe chaos, which can be expected in the dynamics of the full system for parameter values in the vicinity of those presented here.

[4]The existence of horseshoe chaos actually requires the fulfillment of additional conditions on the eigenvalues of the Jacobian matrix of the saddle-focus fixed point (see theorem 5.1 in [36]). The first condition is that the positive real eigenvalue be larger in magnitude than the negative real part of the complex conjugate eigenvalues. This requirement is satisfied here because the real eigenvalues describing the flow in the directions transverse to $\mathscr{M}_\xi$ are $O(1)$, and the complex conjugate eigenvalues describing the flow in the directions parallel to $\mathscr{M}_\xi$ are $O(\xi) \ll 1$. The second condition—that the two real eigenvalues differ in magnitude—can be easily verified as well.

ACKNOWLEDGMENTS

E.K. and R.L. thank Mike Cross and Steve Shaw for fruitful discussions. We are also grateful to Steve Wiggins for his comments on an earlier draft of this manuscript. This work was supported by the US-Israel Binational Science Foundation (BSF) through Grant No. 2004339, by the German-Israeli Foundation (GIF) through Grant No. 981-185.14/2007, and by the Israeli Ministry of Science and Technology.

APPENDIX : EXPLICIT CALCULATION OF THE MELNIKOV INTEGRAL

We integrate here each of the terms in the Melnikov integrand (29). From Eq. (19), owing to the fact that on the homoclinic orbits $J(\pm\infty)=0$, the first of these yields,

$$\int_{-\infty}^{\infty}\frac{d\tilde{H}_1}{dT}dT=-\frac{3rI^rh}{2}\left[\cos 2\phi(\infty)-\cos 2\phi(-\infty)\right]$$
$$=-\frac{3rI^rh}{2}\left[\cos 2(\phi_0+\Delta\phi/2)-\cos 2(\phi_0-\Delta\phi/2)\right]=3rI^rh\sin 2\phi_0\sin\Delta\phi, \tag{A1}$$

where we recall that $\Delta\phi=\phi(\infty)-\phi(-\infty)$. The second term in (29) immediately yields $-3\gamma I^r\Delta\phi$. For the third term in (29) we use Eq. (13), which on resonance yields

$$\int_{-\infty}^{\infty}J\frac{d\chi_1}{dT}dT=\frac{1-r^2}{2r}\int_{-\infty}^{\infty}J^2dT=(1-r^2)2ra^3\left(\frac{2p}{(p^2-q^2)^{3/2}}\operatorname{arctanh}\sqrt{\frac{p-q}{p+q}}+\frac{1}{q^2-p^2}\right)\equiv\Delta\sigma. \tag{A2}$$

For the fourth and last term in (29) we use Eq. (11) and get

$$\int Jd\theta=I^r\theta+\frac{I^r(r^2-1)-2r\Omega_1}{(r-1)\sqrt{r^2-6r+1}}\arctan\left(\frac{r-1}{\sqrt{r^2-6r+1}}\tan\theta\right), \tag{A3}$$

and after substituting the limits, using Eq. (14b), we get

$$\int Jd\theta=I^r\Delta\theta-2\frac{I^r(r^2-1)-2r\Omega_1}{(r-1)\sqrt{r^2-6r+1}}\arctan\left(\frac{r-1}{\sqrt{r^2-6r+1}}\sqrt{\frac{I^r(r-3)-\Omega_1}{I^r(1-r)+\Omega_1}}\right)\equiv I^r\Delta\theta+\Delta\mu. \tag{A4}$$

[1] M. L. Roukes, Sci. Am. **285**, 42 (2001).
[2] A. Cleland, *Foundations of Nanomechanics* (Springer, Berlin, 2003).
[3] H. G. Craighead, Science **290**, 1532 (2000).
[4] D. Rugar, R. Budakian, H. J. Mamin, and B. W. Chui, Nature (London) **430**, 329 (2004).
[5] B. Ilic, H. G. Craighead, S. Krylov, W. Senaratne, C. Ober, and P. Neuzil, J. Appl. Phys. **95**, 3694 (2004).
[6] Y. T. Yang, C. Callegari, X. L. Feng, K. L. Ekinci, and M. L. Roukes, Nano. Lett. **6**, 583 (2006); M. Li, H. X. Tang, and M. L. Roukes, Nature Nanotechnology **2**, 114 (2007); A. K. Naik, M. S. Hanay, W. K. Hiebert, X. L. Feng, and M. L. Roukes, *ibid.* **4**, 445 (2009).
[7] K. Schwab, E. A. Henriksen, J. M. Worlock, and M. L. Roukes, Nature (London) **404**, 974 (2000).
[8] E. M. Weig, R. H. Blick, T. Brandes, J. Kirschbaum, W. Wegscheider, M. Bichler, and J. P. Kotthaus, Phys. Rev. Lett. **92**, 046804 (2004).
[9] M. D. LaHaye, O. Buu, B. Camarota, and K. C. Schwab, Science **304**, 74 (2004); A. Naik, O. Buu, M. D. LaHaye, A. D. Armour, A. A. Clerk, M. P. Blencowe, and K. C. Schwab, Nature (London) **443**, 193 (2006); T. Rocheleau, T. Ndukum, C. Macklin, J. B. Hertzberg, A. A. Clerk, and K. C. Schwab, *ibid.* **463**, 72 (2010).
[10] A. D. O'Connell *et al.*, Nature (London) **464**, 697 (2010).
[11] R. Vijay, M. H. Devoret, and I. Siddiqi, Rev. Sci. Instrum. **80**, 111101 (2009).
[12] R. Lifshitz and M. C. Cross, in *Review of Nonlinear Dynamics and Complexity*, Vol. 1, edited by H. G. Schuster (Wiley, Meinheim, 2008), pp. 1–52.
[13] J. F. Rhoads, S. W. Shaw, and K. L. Turner, J. Dyn. Syst., Meas., Control **132**, 034001 (2010).
[14] K. L. Turner, S. A. Miller, P. G. Hartwell, N. C. MacDonald, S. H. Strogatz, and S. G. Adams, Nature (London) **396**, 149 (1998).
[15] S. Zaitsev, R. Almog, O. Shtempluck, and E. Buks, in *Proceedings of the 2005 International Conference on MEMS, NANO, and Smart Systems (ICMENS 2005)* (IEEE Computer Society, Washington, DC, 2005), pp. 387–391.
[16] J. S. Aldridge and A. N. Cleland, Phys. Rev. Lett. **94**, 156403 (2005).
[17] I. Kozinsky, H. W. C. Postma, O. Kogan, A. Husain, and M. L. Roukes, Phys. Rev. Lett. **99**, 207201 (2007).
[18] E. Buks and M. L. Roukes, J. Microelectromech. Syst. **11**, 802 (2002).
[19] M. Sato, B. E. Hubbard, and A. J. Sievers, Revs. Mod. Phys. **78**, 137 (2006); M. Sato and A. J. Sievers, Phys. Rev. Lett. **98**, 214101 (2007); Low Temp. Phys. **34**, 543 (2008).

[20] D. V. Scheible, A. Erbe, R. H. Blick, and G. Corso, App. Phys. Lett. **81**, 1884 (2002).
[21] B. E. DeMartini, H. E. Butterfield, J. Moehlis, and K. L. Turner, J. Microelectromech. Syst. **16**, 1314 (2007).
[22] R. B. Karabalin, M. C. Cross, and M. L. Roukes, Phys. Rev. B **79**, 165309 (2009).
[23] N. Kacem, S. Hentz, D. Pinto, B. Reig, and V. Nguyen, Nanotechnology **20**, 275501 (2009); N. Kacem, J. Arcamone, F. Perez-Murano, and S. Hentz, J. Micromech. Microeng. **20**, 045023 (2010).
[24] W. Zhang, R. Baskaran, and K. L. Turner, Sensors and Actuators A **102**, 139 (2002).
[25] E. Buks and B. Yurke, Phys. Rev. E **74**, 046619 (2006).
[26] D. S. Greywall, B. Yurke, P. A. Busch, A. N. Pargellis, and R. L. Willett, Phys. Rev. Lett. **72**, 2992 (1994).
[27] M. C. Cross, A. Zumdieck, R. Lifshitz, and J. L. Rogers, Phys. Rev. Lett. **93**, 224101 (2004); M. C. Cross, J. L. Rogers, R. Lifshitz, and A. Zumdieck, Phys. Rev. E **73**, 036205 (2006).
[28] I. Katz, A. Retzker, R. Straub, and R. Lifshitz, Phys. Rev. Lett. **99**, 040404 (2007); I. Katz, R. Lifshitz, A. Retzker, and R. Straub, New J. Phys. **10**, 125023 (2008).
[29] S. Liu, A. Davidson, and Q. Lin, J. Micromech. Microeng. **14**, 1064 (2004).
[30] S. K. De and N. R. Aluru, Phys. Rev. Lett. **94**, 204101 (2005).
[31] K. Park, Q. Chen, and Y.-C. Lai, Phys. Rev. E **77**, 026210 (2008).
[32] H. S. Haghighi and A. H. Markazi, Communications in Nonlinear Science and Numerical Simulation **15**, 3091 (2010).
[33] S. Wiggins, *Global Bifurcations and Chaos—Analytical Methods* (Springer, Berlin, 1988).
[34] V. K. Melnikov, Trans. Mosc. Math. Soc. **12**, 1 (1963).
[35] P. J. Holmes and J. E. Marsden, Commun. Math. Phys. **82**, 523 (1982); J. Math. Phys. **23**, 669 (1982).
[36] G. Kovačič and S. Wiggins, Physica D **57**, 185 (1992); G. Kovačič, Phys. Lett. A **167**, 143 (1992); SIAM J. Math. Anal. **26**, 1611 (1995).
[37] L. P. Šilnikov, Math. USSR Sb. **10**, 91 (1970).
[38] H. B. Chan and C. Stambaugh, Phys. Rev. Lett. **99**, 060601 (2007).
[39] H. B. Chan, M. I. Dykman, and C. Stambaugh, Phys. Rev. Lett. **100**, 130602 (2008).
[40] R. B. Karabalin, X. L. Feng, and M. L. Roukes, Nano Lett. **9**, 3116 (2009).
[41] R. Lifshitz and M. C. Cross, Phys. Rev. B **67**, 134302 (2003).
[42] Y. Bromberg, M. C. Cross, and R. Lifshitz, Phys. Rev. E **73**, 016214 (2006); E. Kenig, R. Lifshitz, and M. C. Cross, *ibid.* **79**, 026203 (2009); E. Kenig, B. A. Malomed, M. C. Cross, and R. Lifshitz, *ibid*. **80**, 046202 (2009).
[43] E. Meron and I. Procaccia, Phys. Rev. Lett. **56**, 1323 (1986); Phys. Rev. A **34**, 3221 (1986).
[44] Z. C. Feng and P. R. Sethna, J. Fluid Mech. **199**, 495 (1989); Nonlinear Dynamics **4**, 389 (1993); Z. Feng and S. Wiggins, Z. Angew. Math. Phys. **44**, 201 (1993); Z. C. Feng and L. G. Leal, J. Appl. Mech. **62**, 235 (1995).
[45] W. Zhang, J. Sound Vib. **239**, 1013 (2001).
[46] J. Moehlis, J. Porter, and E. Knobloch, Physica D **238**, 846 (2009).
[47] T. J. Kaper and G. Kovačič, Trans. Am. Math. Soc. **348**, 3835 (1996).
[48] G. Haller and S. Wiggins, Arch. Ration. Mech. Anal. **130**, 25 (1995).